Decomposition of pentaerythritol tetranitrate [$C(CH_2ONO_2)_4$] following electronic excitation

Zijun Yu and Elliot R. Bernstein

Citation: The Journal of Chemical Physics **135**, 154305 (2011); doi: 10.1063/1.3652893
View online: http://dx.doi.org/10.1063/1.3652893
View Table of Contents: http://aip.scitation.org/toc/jcp/135/15
Published by the American Institute of Physics

Decomposition of pentaerythritol tetranitrate [$C(CH_2ONO_2)_4$] following electronic excitation

Zijun Yu and Elliot R. Bernstein[a)]
Department of Chemistry, Colorado State University, Fort Collins, Colorado 80523, USA

(Received 15 July 2011; accepted 28 September 2011; published online 20 October 2011)

We report the experimental and theoretical study of the decomposition of gas phase pentaerythritol tetranitrate (PETN) [$C(CH_2ONO_2)_4$] following electronic state excitation. PETN has received major attention as an insensitive, high energy explosive; however, the mechanism and dynamics of the decomposition of this material are not clear yet. The initial decomposition mechanism of PETN is explored with nanosecond energy resolved spectroscopy and quantum chemical theory employing the ONIOM algorithm at the complete active space self-consistent field (CASSCF) level. The nitric oxide (NO) molecule is observed as an initial decomposition product from PETN at three UV excitation wavelengths (226, 236, and 248 nm) with a pulse duration of 8 ns. Energies of the three excitation wavelengths coincide with the (0–0), (0–1), and (0–2) vibronic bands of the NO $A\ ^2\Sigma^+ \leftarrow X\ ^2\Pi$ electronic transition, respectively. A unique excitation wavelength independent dissociation channel is observed for PETN, which generates the NO product with a rotationally cold (∼20 K) and a vibrationally hot (∼1300 K) distribution. Potential energy surface calculations at the ONIOM(CASSCF:UFF) level of theory illustrate that conical intersections play an important role in the decomposition mechanism. Electronically excited S_1 PETN returns to the ground state through the $(S_1/S_0)_{CI}$ conical intersection, and undergoes a nitro-nitrite isomerization to generate the NO product. © *2011 American Institute of Physics*. [doi:10.1063/1.3652893]

I. INTRODUCTION

Energetic material pentaerythritol tetranitrate (PETN) [$C(CH_2ONO_2)_4$] has been the focus of attention for decades due to its numerous applications in the explosive core of industrial detonating fuses, in the base charge of commercial blasting caps, in industrial boosters, in linear shaped charges, and in commercial and military detonators.[1,2] It is also used as a vasodilator drug to treat certain heart conditions, such as for management of angina.[3] Thus, PETN has intensively been investigated both experimentally and theoretically.[4–11]

Swayambunathan *et al*.[4] have performed laser photofragmentation fragment detection (PF-FD) experiments near 227 nm to detect trace concentrations of PETN. In their experiments, detection is accomplished by resonance enhanced multiphoton ionization with miniature electrodes and by laser-induced fluorescence with a photodetector: a nitric oxide (NO) fragment is found to be the major product. Using a nanosecond time-resolved spectropyrometric system operated at six discrete wavelengths between 350 and 700 nm, shock temperatures of PETN single crystals have been measured by Yoo *et al*.[5] The results show that the shock sensitivity of PETN is strongly dependent on crystal orientation: sensitive along shock propagation normal to the (110) plane, but highly insensitive to it normal to the (100) plane. The detonation temperature of PETN is, however, independent of crystal orientation. Wu and co-workers[6] have performed semi-empirical quantum mechanical molecular dynamics (MD) simulations involving collisions of two PETN molecules at different molecular orientations and at several intermolecular separations. They point out that the dissociation mechanism of PETN remains unimolecular, and the role of binary collisions is to transfer the kinetic energy to excite internal degrees of freedom in PETN molecules; the dominant initial reaction path during binary collision involves the bond breaking of an O–NO_2 group. This dissociation mechanism is insensitive to mutual molecular orientations and is identical to the lowest energy pathway for unimolecular reactions involving an isolated PETN molecule. The probability of collision -induced decomposition of PETN depends strongly on initial conditions, however, in agreement with the experimentally observed sensitivity of shock initiated detonation in bulk PETN along different crystalline orientations. However, the detailed mechanism of energy transfer from the binary collision to vibrational modes that leads to unimolecular dissociation has not been studied. Landerville *et al*.[7] performed Born-Oppenheimer direct dynamics classical trajectory simulations of bimolecular collisions of PETN molecules to investigate the fundamental mechanisms of hypervelocity chemistry relevant to initiating reactions immediately behind the shock wavefront in energetic molecular crystals. The reactive case simulations show the formation of NO_2 as the dominant reaction pathway in all cases, with H_2CO formation for cases in which a large amount of collision energy is localized in a particular arm of the molecule. Bond dissociation energies play a significant role in the decomposition mechanism.

Studies of PETN chemistry have appeared for crystal thermal decomposition and stability,[4–11] but little information

a)Author to whom correspondence should be addressed. Electronic mail: erb@lamar.Colostate.edu.

 © 2011 American Institute of Physics

is available for unimolecular, isolated molecule decomposition of PETN. Additionally, ignition processes involving sparks, shock, slow/rapid heating, lasers, and arcs can all initiate the decomposition reaction of PETN by generating excited electronic states. Thus, investigations of the gas phase, isolated molecule decomposition of PETN following electronic excitation will yield an improved understanding of the initial decomposition mechanisms and dynamics for $NO/NO_2/NO_3$ containing energetic materials, at a fundamental level.

In this work, we will focus on understanding the decomposition mechanism and dynamics of PETN under unimolecular conditions. Nanosecond energy resolved spectroscopy is employed to investigate the excited electronic state decomposition mechanisms and dynamics of isolated gas phase PETN. The PETN parent molecule is excited to its (n,π^*) excited electronic state by absorption of a single UV photon and a dissociation product, nitric oxide, is observed by a one color (1+1) resonance enhanced two photon ionization (R2PI) scheme using time of flight mass spectrometry (TOFMS) detection. Three vibronic transitions $A\,^2\Sigma^+(\upsilon' = 0) \leftarrow X\,^2\Pi(\upsilon'' = 0,1,2)$ of the NO product molecule from PETN are observed: the NO product from PETN is generated through an excitation wavelength independent, nonadiabatic, dissociation channel and is characterized by a rotationally cold (~20 K) and a vibrationally hot (~1300 K) internal energy distribution. Quantum mechanical calculations [ONOIM (CASSCF:UFF)] are performed on ground and electronic excited states of PETN in order to generate details about the decomposition mechanisms pertaining to PETN. Based on these calculations and the experimental observations, we propose that PETN from the S_1 state goes back to the S_0 state through a nonadiabatic mechanism involving a $(S_1/S_0)_{CI}$ conical intersection (CI) and, then, undergoes a nitro-nitrate isomerization on the S_0 potential energy surface (PES), finally giving birth to the NO product. Therefore, present results provide several detailed insights into the unimolecular decomposition behavior of PETN from its excited electronic states. We note that a number of other $NO/NO_2/NO_3$ containing energetic materials (such as, 1,3,5-trinitroperhydro-1,3,5-triazine (RDX), octahydro-1,3,5,7-tetranitro-1,3,5,7-tetrazocine (HMX), 2,4,6,8,10,12-Hexanitro-2,4,6,8,10,12-hexaazaisowurtzitane (CL20) and 3,3′-diamino-4,4′-azoxyfurazan (DAAF)) (Refs. 12–14) follow a very similar decomposition mechanism from their electronic excited states.

II. EXPERIMENTAL PROCEDURE

A detailed experimental procedure for nanosecond mass resolved excitation spectroscopy has been described in our previous publications.[15,16] Briefly, the experimental setup consists of laser systems with nanosecond time duration pulses (10 Hz), a supersonic jet expansion nozzle with a laser desorption attachment, and a time of flight mass spectrometer vacuum chamber. For the nanosecond laser experiments, a single pump-probe laser beam at three separate wavelengths (226, 236, and 248 nm) is used both to initiate dissociation of PETN molecules and to detect NO following a one-color (1+1) R2PI scheme ($A\,^2\Sigma^+(\upsilon' = 0) \leftarrow X\,^2\Pi(\upsilon'' = 0,1,2)$ and $I \leftarrow A$ transitions) through TOFMS. The three UV laser wavelengths used in the nanosecond laser experiments are generated by a pulsed dye laser, pumped by the second harmonic (532 nm) of a neodymium doped yttrium aluminum garnet laser's fundamental output (1.064 μm), in conjunction with a nonlinear wavelength extension system. The typical pulse energy of the UV laser is 50–400 μJ/pulse depending on the exact wavelength of interest for a one-color experiment, which gives a laser beam intensity (I) ~ (0.3–2.5) × 10^7 W/cm^2 for a 8 ns pulse duration at a focused beam diameter of 0.5 mm.

The isolated gas phase PETN molecules are produced through a combination of matrix-assisted laser desorption and supersonic jet expansion. The nozzle employed for the sample beam generation is constructed from a Jordan Co. pulsed valve and a laser desorption attachment.[15] Sample drums for matrix desorption are prepared by wrapping a piece of porous filter paper around a clean aluminum drum. A solution of equimolar amounts of sample and matrix (R6G dye) in acetone is uniformly sprayed on the sample drum. An air atomizing spray nozzle (Spraying System Co.) with siphon pressure of 10 psi is used to deposit the PETN and R6G on the drum surface. During the spraying, the drum is rotated and heated with a halogen lamp to make sure that the coating is homogeneous and dry. The dried sample drum is then placed in the laser ablation head/nozzle assembly and put into a vacuum chamber. In order to maintain a fresh sample area for each laser ablation shot, a single motor is used to rotate and translate the sample drum simultaneously. PETN molecules are desorbed from the drum by laser ablation at 532 nm, entrained in the flow of helium carrier gas through a 2 × 60 mm channel in the ablation head, and expanded into the vacuum chamber.[17,18]

The experiment is run at a repetition rate of 10 Hz. The timing sequence for the pulsed nozzle, ablation laser, and ionization laser is controlled by a time delay generator (SRS DG535). The molecular beam is perpendicularly crossed by a UV laser beam that is focused to a spot size of about 0.5 mm at the ionization region of a time of flight mass spectrometer. A background pressure of 2 × 10^{-6} Torr is maintained in the vacuum chamber during the experiment. Ion signals are detected by a microchannel plate detector. Signals are recorded and processed on a personal computer using a boxcar averager (SRS SR 250) and an analog-to-digital conversion card (Analog Devices RTI-800).

III. COMPUTATIONAL METHOD

The ONIOM method, which divides a large molecular system into two or three layers and treats them with different levels of theory and, then, combines those results into the final predictions, is used to execute the calculation for the large molecular system PETN. In our previous work,[19] the ONIOM (CASSCF:UFF) method has been employed to explore the nonadiabatically coupled ground and excited electronic state PESs of the isolated RDX molecule. In that calculation, one of the N–NO_2 moieties of the RDX molecule is considered to be an active site. Electronic excitation of RDX is supposed to be localized in the active site, which is treated with the CASSCF method. The remainder of the molecule was calculated by

a universal force field (UFF)/molecular mechanics (MM) or Hartree-Fock (HF)/quantum mechanics (QM) method to obtain the steric and electrostatic influences on the active site. Computational results predict that a nitro-nitrite isomerization on the S_0 PES is the major decomposition channel for the electronic excited RDX molecule. Nitro-nitrite isomerization of RDX is found to occur through a series of conical intersections and is finally predicated to produce rotationally cold but vibrationally hot distributions of NO products: this decomposition pathway is in good agreement with the experimental observation of rovibrational distributions of the NO product. Thus, this previous work[19] indicates that the ONIOM method combined with the CASSCF method is a feasible means to explore the excited electronic state PESs for large energetic molecules.

In current work, we use the GAUSSIAN 09 package[20] installed on the Ember (NCSA, TeraGrid)) supercomputer to perform the ONIOM calculation. In this calculation, we consider two layer QM:MM combinations, for which the total energy of a molecule is expressed through an extrapolation scheme as

$$E^{\mathrm{ONIOM}} = E^{\mathrm{High}}_{\text{active site}} + E^{\mathrm{Low}}_{\mathrm{real}} - E^{\mathrm{Low}}_{\text{active site}}.$$

Here, active site stands for a small part of the real molecule, at which a chemical or physical process being studied is localized. An adequate high level is employed to describe accurately the behavior of the active site. A low level and cheaper MM method is employed for the full molecule (denoted as real). As a consequence, the active site is treated with both high and low levels of theory, and the full molecule is treated with only a low level of theory. The energy gradient is the derivative of the above expression with respect to the reaction coordinate, and the optimization is performed on the total PES gradient. The $(E^{\mathrm{Low}}_{\mathrm{real}} - E^{\mathrm{Low}}_{\text{active site}})$ term in the ONIOM energy expression describes both the contribution from the low level region and the interaction between the high and low level regions. In other words, coupling between the two regions is evaluated at a low computational level of theory. In general, the ONIOM method cannot calculate the absolute energy of the real system, as the various subcalculations (MM) either have different energy scales or are less accurate on the same energy scale (pure QM); however, the energy difference between two points on a PES will be reproduced with considerable accuracy.[21–23]

The active site and the remainder of the PETN molecule considered for the present work are illustrated in Fig. 1. The high level region is depicted by balls, and the low level region is depicted by a wire frame. Here, electronic excitation is assumed to be localized entirely in the active site (more specifically in one O–NO_2 unit) of the molecule. The CASSCF algorithm (to calculate $E^{\mathrm{High}}_{\text{active site}}$) is selected to treat the active site because this approach can successfully describe excited electronic states with adequate accuracy. Choice of a low level method (to calculate $E^{\mathrm{Low}}_{\mathrm{real}} - E^{\mathrm{Low}}_{\text{active site}}$) is not straightforward, however. Based on the assumption that electronic excitation is completely localized in the high level region (active site), one can choose a ground state method (e.g., HF, UFF), because the electronic excitation is the same in $E^{\mathrm{Low}}_{\mathrm{real}}$ and $E^{\mathrm{Low}}_{\text{active site}}$ and, therefore, cancels in the difference $(E^{\mathrm{Low}}_{\mathrm{real}} - E^{\mathrm{Low}}_{\text{active site}})$.

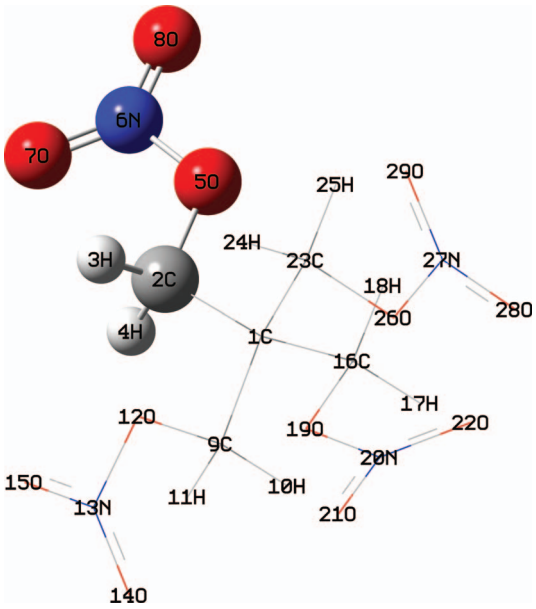

FIG. 1. Optimized structure of PETN at ONIOM(CASSCF(6,6)/6-31G(d):UFF) level of theory on the ground state. The high-level region of PETN is depicted by balls, and the low-level region is depicted by a wire frame.

For the present study, low level ground state methods, such as UFF MM, are employed for calculation of the properties of the remainder of the PETN molecule. The difference of interaction energies between the high and low level regions related to the ground and excited electronic-state structures of PETN is assumed to be negligible.[24]

To explore the excited state potential energy surfaces, the active space comprises 6 electrons distributed in 6 orbitals, denoted as CASSCF(6,6). Orbitals used in the active space are one nonbonding n_O orbital, one NO bonding orbital σ_{NO}, one π-bonding orbital π_O, one ONO π-antibonding orbital π_{ONO}*, one NO antibonding orbitals σ_{NO}*, and one NO_2 antibonding orbitals σ_{ONO}*, as illustrated in Fig. 2. Search for critical points (minima, transition states (TSs), and CIs) on excited electronic and ground state PESs for PETN is performed at the ONIOM[CASSCF(6,6)/6-31G(d):UFF] level of theory with the GAUSSIAN 09 program. No symmetry restrictions are applied during the calculations. Vertical excitation energies are computed by state averaging over the ground state and two singlet excited states with equal weights. The geometries of the critical points are optimized with state averaging over the S_0 and S_1 states with equal weights. Transition state structures are characterized by analytical frequency calculations. Equilibrium geometry calculations are conducted taking the total charge as neutral and the spin multiplicity as 1. The whole potential energy surfaces are calculated using an intrinsic reaction coordinate (IRC) algorithm and a SCAN algorithm implemented in GAUSSIAN 09.

IV. EXPERIMENTAL RESULTS

The PETN parent molecule is excited to an upper vibronic state by absorption of a single UV photon: three different excitation wavelengths (226, 236, and 248 nm) are employed. The parent molecule decomposes into products

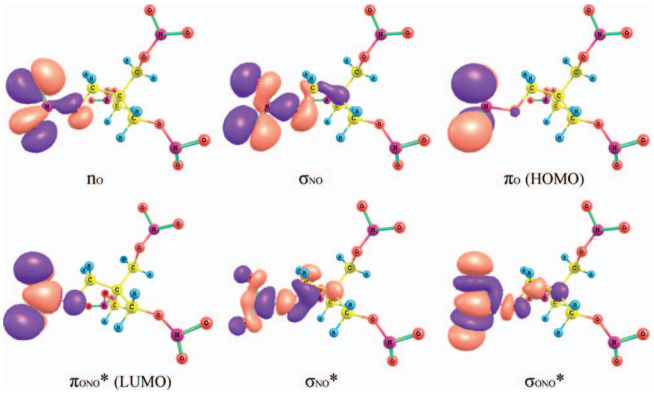

FIG. 2. Orbitals used in active space for CASSCF calculation for PETN.

through specific decomposition pathways. Different possible decomposition pathways of the PETN parent molecule are illustrated in Fig. 3. The PETN molecule potentially can generate a number of initial products, such as, NO after nitro-nitrite isomerization, NO_2 and ONO_2 through direct N–O or C–O bond rupture, and HONO elimination. In the experiments, however, NO is observed to be the major initial dissociation product in the decomposition of the electronic excited PETN molecule. The NO product is probed using a one color (1+1) R2PI detection scheme through TOFMS. The three excitation wavelengths used in this work also correspond to the resonance (0–0), (0–1), and (0–2) vibronic bands of the $A\ ^2\Sigma^+ \leftarrow X\ ^2\Pi$ electronic transitions of the NO product, respectively. By scanning the nanosecond laser excitation wavelength, a (1+1) R2PI rotationally resolved spectrum of the NO product from different parent molecules is obtained. The parent molecule has continuous absorption in these wavelength regions.

The (1+1) R2PI spectra of the three vibronic transitions, $A\ ^2\Sigma^+(\upsilon' = 0) \leftarrow X\ ^2\Pi(\upsilon'' = 0,1,2)$ of the NO product observed from the decomposition of the electronic excited PETN molecule are shown in Fig. 4. The most intense feature in each spectrum of NO can be assigned as the $(Q_{11}+P_{12})$ band head of each vibronic band,[25,26] and the less intense features within each spectrum are due to other rovibronic transitions. Spectral simulations based on Boltzmann population distributions for the three vibronic transitions produce similar

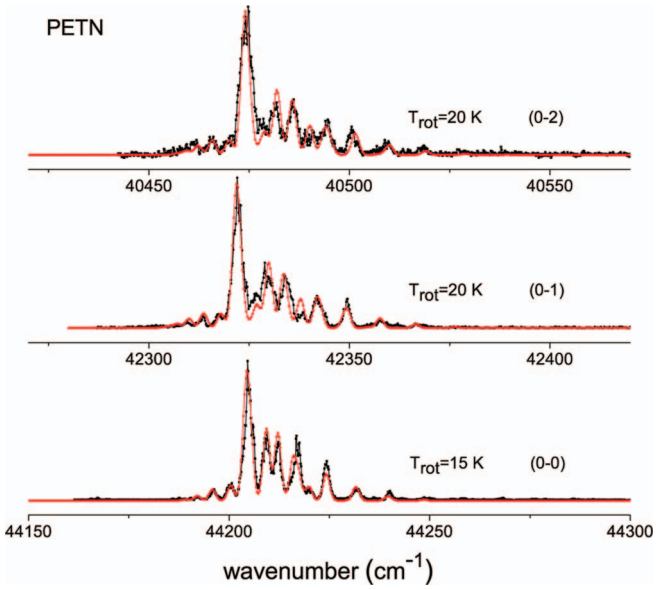

FIG. 4. One color (1+1) R2PI spectra of the vibronic transitions $A\ ^2\Sigma^+(\upsilon' = 0) \leftarrow X\ ^2\Pi(\upsilon'' = 0,1,2)$ of the NO product from the decomposition of the electronically excited PETN molecule. Rotational temperature simulations with a Boltzmann population distribution show that the three observed vibrational levels of the ground electronic state have a cold rotational temperature of ~20 K.

rotational temperatures (~20 K). The vibrational temperature of the NO product from PETN can also be obtained by simulating the relative intensities among the observed vibronic bands using a Boltzmann population distribution analysis and Franck-Condon factors. By comparing the experimental data with simulations at different vibrational temperatures, the vibrational temperature of the NO product from PETN is estimated to be ~1300 K.

The NO product from decomposition of PETN is generated following single photon absorption. This is confirmed by careful analysis of the linewidth of the NO mass peak. Extra kinetic energy from photodissociation following multiphoton absorption would generate additional linewidth for product mass channels. Moreover, if the PETN molecule absorbs multiple photons at 226 nm sequentially, it can photodissociate (fragment) into NO following ionization. This will also lead to a broadening of the linewidth of the NO

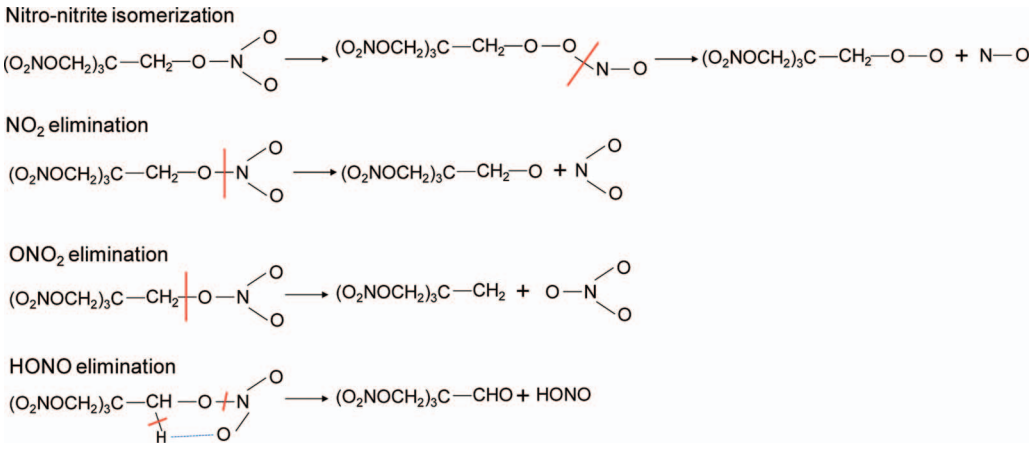

FIG. 3. Different possible decomposition channels for PETN.

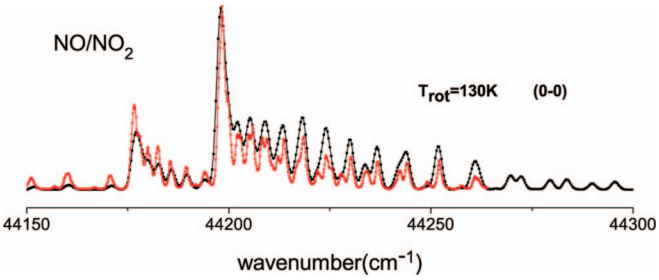

FIG. 5. One color (1+1) R2PI spectra of the vibronic transitions $A\ ^2\Sigma^+(\upsilon' = 0) \leftarrow X\ ^2\Pi(\upsilon'' = 0)$ of the NO product from the decomposition of the electronically excited NO_2. Rotational temperature is estimated to be ~130 K.

mass signal. The linewidth of the NO mass channel signal is observed to be about 10 ns, which is the instrumental linewidth of our laser/TOFMS setup. Therefore, we believe that the NO product is associated with a single photon absorption by these molecules. Furthermore, the laser energy is reduced to ~100 μJ/pulse, so that the multiphoton dissociation of PETN is avoided. Hot PETN parent molecules that can be generated in the matrix-assisted laser desorption (MALD) process would be effectively relaxed and cooled in the highly collisional expansion environment through the supersonic nozzle.

Although the MALD technique is a good method to place easily fragmented, fragile molecules in the gas phase without fragmentation, a great effort is taken in our previous and present work to ensure that the sample molecules are not fragmented in the ablation process.[15,16] Three different methods have been employed to explore this issue: comparison of NO velocity distributions from the nozzle, determination of arrival time for the NO signal intensity as a function of nozzle/pump laser timing, and NO rotational and vibrational temperature determinations as a function of NO source. These methods demonstrate that NO from PETN is generated at the ionization region of the TOFMS, not in the laser desorption region of the nozzle.

The (1+1) R2PI spectrum of NO from photolysis of NO_2 in the NO $A\ ^2\Sigma^+(\upsilon' = 0) \leftarrow X\ ^2\Pi(\upsilon'' = 0)$ transition region is presented in Fig. 5. The (0–0) vibronic band of the NO product is observed from photolysis of NO_2 gas at 226 nm photoexcitation: the spectrum is characterized by a rotational temperature of about 130 K. Comparing the rotational distribution of NO from NO_2 gas and PETN, NO_2 is excluded from the primary source for NO and the major reaction channel for the decomposition of electronically excited PETN, since if NO_2 loss were the major reaction channel for decomposition of electronically excited PETN, NO_2 would subsequently dissociate to NO in the wavelength range used in our experiments, and thus NO from NO_2 produced by PETN should present similar or hotter rotational distributions compared to that from expansion cooled NO_2 gas. NO from photolysis of the PETN molecule is, however, rotationally colder than that from expansion cooled NO_2 gas, which indicates that NO_2 cannot be the precursor for the NO product and the major reaction channel in the decomposition of the electronically excited PETN molecule. Instead, a nitro-nitrite isomerization channel is proposed to be the mechanism of NO elimination from the PETN molecule. With regard to the HONO reaction channel, we have determined that the HONO elimination in all X–NO_2 system is less than 5% of the NO elimination following the nitro-nitrite isomerization in previous work.[16,27,28] So, we have not presented this channel here as a major competitor for the nitro-nitrite isomerization/NO elimination channel. The detailed description of different reaction channels for X–NO_2 systems including models and energetic systems will be discussed in a future paper.

V. THEORETICAL RESULTS

A. Equilibrium geometry of PETN

The optimization of PETN on the ground state using the two layer ONIOM methodology described in Sec. III is conducted by using the CASSCF method with a 6-31G(d) basis set for the high level region and UFF for the low level region. The optimized Frank-Condon (FC) geometry of PETN on the ground state is shown in Fig. 1. PETN has a number of conformers. Here, only the conformer belonging to point group S_4 is chosen to execute the ONIOM combined with CASSCF methodology to explore the potential energy surfaces of PETN, since the S_4 point group structure of PETN is the most stable conformer.[29] In general, with a good combination of theory levels for the active site and the low level region of the molecule for an ONIOM methodology, the predicted geometrical parameters should be similar to those predicted by a pure quantum mechanical calculation. Therefore, a comparison of geometrical parameters of PETN predicted at the ONIOM(CASSCF/6-31G(d):UFF) and MP2/6-31G(d) levels of theory is also performed to judge appropriateness of the CASSCF:UFF combination used in the present ONIOM methodology. Note that comparison of geometrical parameters for PETN predicted at the ONIOM(CASSCF:UFF) and pure quantum mechanical CASSCF levels of theory is impossible to perform because the PETN molecule is too large to be treated with a pure CASSCF multiconfiguration SCF level of theory. The geometrical parameters for PETN computed at the MP2/6-31G(d) and ONIOM(CASSCF(6,6)/6-31G(d):UFF) levels of theory are given in Table I (for atom labels, see Fig. 1). The agreement between the ONIOM(CASSCF:UFF) and MP2 results for the active site of PETN is excellent, in general. This suggests that the CASSCF:UFF combination in the ONIOM algorithm is an adequate method to predict the structure of PETN, and even more to explore the potential energy surfaces of PETN.

B. Electronic transition of PETN

The vertical excitation energies for PETN, computed at the ONIOM(CASSCF(6,6)/6-31G(d):UFF) optimized Franck-Condon geometry (i.e., the ground state minimum) are listed in Table II (the calculated energies have not been corrected for zero point energy). The calculated vertical excitation energies of 4.9 ev for S_1 and 6.0 ev for S_2 are in agreement with the experimental UV-Vis absorption maxima of 4.8 and 6.5 ev, which is shown in Fig. 6. CASSCF calculations show that the two lowest lying excited states for

TABLE I. Geometrical parameters of PETN at MP2/6-31G(d) and ONIOM(CASSCF(6,6)/6-31G(d):UFF) (for atom labels see Fig. 1).

	MP2	CASSCF
	Bond lengths (Å)	
C_2O_5	1.435	1.426
O_5N_6	1.422	1.345
N_6O_7	1.200	1.193
N_6O_8	1.191	1.186
	Bond angles (°)	
$C_2O_5N_6$	114.1	115.1
$O_5N_6O_7$	116.9	118.6
$O_7N_6O_8$	130.8	127.9
	Dihedral angle (°)	
$C_2O_5N_6O_7$	−0.46	− 0.24

PETN are n → π^* transitions, which is consistent with the results for nitromethane, dimethylnitramine, and RDX, as we have published previously,[19,27,28] even though the HOMO and LUMO orbitals are π and π^* orbitals (see Fig. 2). Both experiments and calculations[30–32] indicate that the electrons excited for the $S_0 \rightarrow S_1$ transitions of these NO_2-containing systems almost exclusively come from the nonbonding orbital n_O of NO_2. These NO_2 localized n → π^* transitions are similar for PETN, nitromehtane, dimethylnitamine, RDX, HMX, etc. In addition, by comparing the three excitation energies (5.49 eV at 226 nm, 5.25 eV at 236 nm, and 5.00 eV at 248 nm) used in the experiment with the calculated vertical excitation energies (4.9 and 6.0 eV) of the S_1 (n,π^*) and S_2 (n,π^*) exited states of the PETN molecule, one can find that the PETN molecule is excited to its S_1 (n,π^*) excited state by these three excitation wavelengths.

C. Electronic PESs of PETN

A schematic one-dimensional plot of the multidimensional singlet PESs (S_0 and S_1) of PETN is presented in Fig. 7. The plot is along the minimum-energy path coordinates available to PETN from the Franck-Condon point on S_1, "S_1/(n,π^*)," with locations and structures of different critical points and CIs. All the structures for the important points labeled in Fig. 7 are presented in Fig. 8. "FC geometry" is the optimized minimum energy structure of PETN on the ground state S_0. "$S_{0,TS}$" is the tight transition state of the nitro-nitrite isomerization on S_0. "$(S_1/S_0)_{CI}$" is the conical intersection between S_0 and S_1: the smallest adiabatic energy gap between the S_0 and S_1 surfaces near the "$(S_1/S_0)_{CI}$" of PETN is computed to be ∼2 cm^{-1}, which suggests that the S_1 and S_0 surfaces are strongly nonadiabatically coupled at this point (CI). "$S_{0,inter}$" is the intermediate structure between

TABLE II. Vertical transition energy (without zero point energy correction) at FC geometry.

Compound	Excited state	E_{cal} (eV)	E_{exp} (eV)
PETN	S_1/(n,π^*)	4.9	4.8
	S_2/(n,π^*)	6.0	6.5

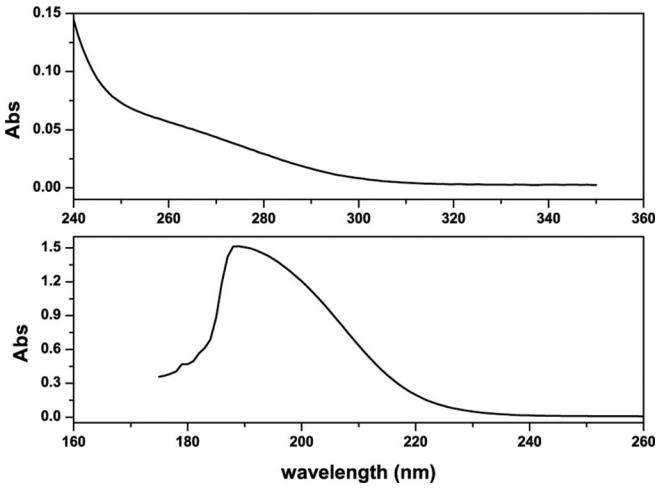

FIG. 6. The UV-Vis absorption spectrum of PETN in acetonitrile.

the tight transition state "$S_{0,TS}$" and the conical intersection "$(S_1/S_0)_{CI}$," which is obtained by IRC from the conical intersection "$(S_1/S_0)_{CI}$." "$S_{0,nitrite}$" is the nitrite structure of PETN after nitro-nitrite isomerization on S_0 and "$S_{0,TS,NO\text{-}elimin}$" is the transition state for NO elimination from the nitrite structure of PETN on S_0. "$S_{1,min}$" is the optimized minimum energy structure of PETN on the first excited state S_1. "$S_{1,TS}$" is the transition state on S_1 between "$S_{1,min}$" and "$(S_1/S_0)_{CI}$" on S_1. "$S_{1,nitrite}$" is the nitrite structure of PETN after nitro-nitrite isomerization on S_1 and "$S_{1,TS,NO\text{-}elimin}$" is the transition state for NO elimination from the nitrite structure of PETN on S_1. "$S_{1,TS,nitro\text{-}nitrite}$" is the transition state between the conical intersection "$(S_1/S_0)_{CI}$" and the nitrite structure

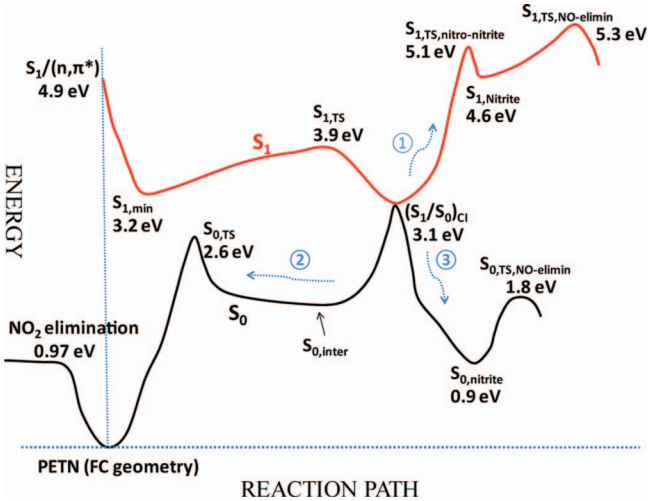

FIG. 7. A schematic one-dimensional projection of the multidimensional potential energy surfaces of PETN computed at ONIOM(CASSCF(6,6)/6-31G(d):UFF) level of theory. The labeled relative CASSCF energies of the critical points (minimum, conical intersection, transition state) on the PESs with respect to the FC geometry (S_0) are not corrected for zero point energy. The potential energy surfaces are calculated by the IRC and SCAN algorithms: the FC geometry and $S_{0,inter}$ are the two minima connected by the transition state $S_{0,TS}$; $S_{0,inter}$ and $S_{0,nitrite}$ are the two minima connected by the conical intersection $(S_1/S_0)_{CI}$; $(S_1/S_0)_{CI}$ and $S_{1,min}$ are the two minima connected by the transition state $S_{1,TS}$; $(S_1/S_0)_{CI}$ and $S_{1,nitrite}$ are the two minima connected by the transition state $S_{1,TS,nitro\text{-}nitrite}$.

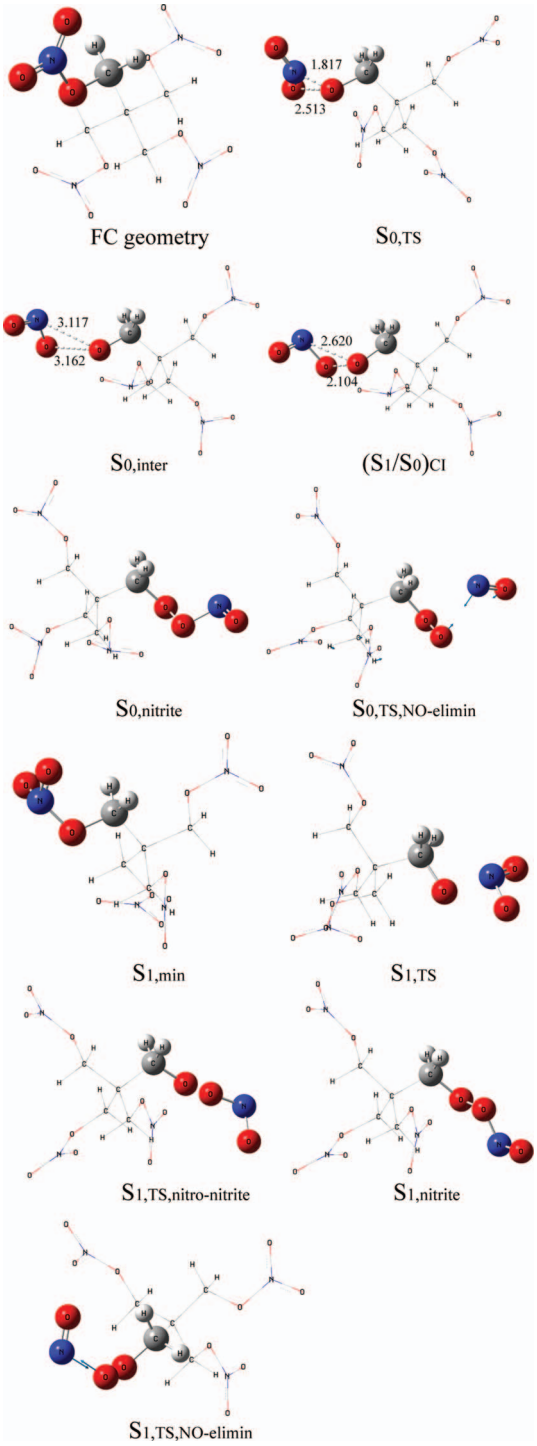

FIG. 8. Structures of PETN at different critical points on PESs calculated at ONIOM[CASSCF(6,6)/6-31G(d):UFF] level of theory. "FC geometry" is the optimized minimum energy structure of PETN on the ground state S_0. "$S_{0,TS}$" is the tight transition state of the nitro-nitrite isomerization on S_0. "$(S_1/S_0)_{CI}$" is the conical intersection between S_0 and S_1. "$S_{0,inter}$" is the intermediate structure between the tight transition state "$S_{0,TS}$" and the conical intersection "$(S_1/S_0)_{CI}$," which is obtained by the IRC from the conical intersection "$(S_1/S_0)_{CI}$." "$S_{1,min}$" is the optimized minimum energy structure of PETN on the first excited state S_1. "$S_{1,TS}$" is the transition state on S_1 between "$S_{1,min}$" and "$(S_1/S_0)_{CI}$" on S_1. "$S_{1,TS,nitro\text{-}nitrite}$" is the transition state between the conical intersection "$(S_1/S_0)_{CI}$" and the nitrite structure of PETN "$S_{1,nitrite}$" on S_1. "$S_{0,nitrite}$" and "$S_{1,nitrite}$" are the nitrite structures of PETN after nitro-nitrite isomerization on S_0 and S_1, respectively. "$S_{0,TS,NO\text{-}elimin}$" and "$S_{1,TS,NO\text{-}elimin}$" are the transition states of NO elimination from the nitrite structure of PETN on S_0 and S_1, respectively. The arrows in the structure of the transition states show the reaction coordinate of the imaginary frequency.

of PETN "$S_{1,nitrite}$" on S_1, which is obtained by searching for a TS between "$(S_1/S_0)_{CI}$" and "$S_{1,nitrite}$" using the CASSCF multireference algorithm. The potential energy surfaces are explored by the IRC and SCAN algorithms, and then they are combined together to build the whole reaction path.

In Fig. 7, the relative CASSCF energies of the critical points (minimum, conical intersection, transition state) on both excited S_1 and ground S_0 PESs of PETN with respect to the energy of ground state FC geometry are also present (the calculated energies have not been corrected for zero point energy). And the blue dotted arrows (labeled 1, 2, 3) in Fig. 7 indicate different possible decomposition channels for the excited state decomposition of PETN along different relevant nuclear coordinates. One decomposition pathway of PETN from the FC point of the S_1 surface would be along the S_1 surface, which bypasses the $(S_1/S_0)_{CI}$ conical intersection, and remains on the S_1 PES (arrow 1). The molecule must then overcome the $S_{1,TS,nitro\text{-}nitrite}$ transition state to initiate the nitro-nitrite isomerization on the S_1 surface. This process, however, requires an activation energy barrier of 2 eV to be surmounted on the S_1 surface of PETN with respect to the $(S_1/S_0)_{CI}$ conical intersection (see Fig. 7). For subsequent NO elimination on the S_1 PES, PETN must surmount the $S_{1,TS,NO\text{-}elimin}$ transition state subsequent to the nitro-nitrite isomerization. Then, the energy barrier to subsequent NO loss is about 0.7 eV with respect to the $S_{1,nitrite}$ local minimum. The unstable normal mode of vibration for the NO elimination transition state on the S_1 surface of PETN clearly shows a large component of force on only the N atom of the eliminated NO (see Fig. 8 "$S_{1,TS,NO\text{-}elimin}$"). This force imbalance is expected to produce considerable torque on the terminal NO moiety. Therefore, decomposition of the molecule through nitro-nitrite isomerization followed by NO elimination on the S_1 surface is expected to produce a rotationally hot NO product. To proceed through this pathway, however, PETN must first surmount a high activation barrier (2 eV) and then a barrier of 0.7 eV on the S_1 surface. Even though the photon energy is about 5.5 eV at 226 nm, which is a little higher than the maximum energy barrier $S_{1,TS,NO\text{-}elimin}$ (5.3 eV with respect to the FC geometry of the ground state), all the photon energy would be required to overcome the energy barriers, without rotation and vibration excitation of the PETN molecule in the dissociation process. Therefore, such high activation barriers on the S_1 PES render the pathway untenable.

Based on the conclusion above, one can find that the decay path, from the S_1 state FC point to the minimum of the S_1 state ($S_{1,min}$), surmounting the energy barrier on the S_1 surface, and finally reaching the $(S_1/S_0)_{CI}$ conical intersection, is the most energetically favorable decomposition pathway for PETN: this pathway will then lead the molecule to its ground state PES. After the molecule comes back to the ground state through $(S_1/S_0)_{CI}$, a number of fragmentation channels are energetically available for PETN. To understand these different possible channels on the ground state PES of PETN, different critical points and related minimum energy paths on the S_0 state of PETN must be explored. Undoubtedly, the overall most favorable path, which is determined by many factors such as the steepest descent and the largest ΔE, from $(S_1/S_0)_{CI}$ would be the primary decomposition channel for

this molecule.[33] A key feature of crossing geometries is that more than one relaxation direction might exist. From calculational results, two most possible energy decay pathways can be identified on the S_0 PES: one involves coming back to FC minimum geometry after surmounting an activation barrier (blue dotted line, arrow 2), and the other involves evolution along the deepest descent path, which results in a nitro-nitrite isomerization (blue dotted line, arrow 3). Before addressing the most favorable path connecting to $(S_1/S_0)_{CI}$ on the ground state, we first point out a number of important insights for the ground state decomposition of PETN.

If the PETN molecule surmounts the activation barrier and goes back to FC minimum geometry after crossing through the $(S_1/S_0)_{CI}$ CI (this is energetically favorable), the dynamical behavior will act as the thermal decomposition of PETN on the ground state PES. The ONIOM(CASSCF:UFF) level of theory predicts activation energies for the O–NO_2 bond dissociation energy barrier from PETN and the NO elimination barrier following nitro-nitrite isomerization of 0.97 and 2.6 eV (see Fig. 8), respectively. Therefore, these results indicate that, if the PETN molecule is thermally dissociated on the ground state surface only, the major decomposition channel should be O–NO_2 bond dissociation because this channel is associated with the lowest activation barrier. In order to elucidate the first chemical events that trigger chemistry behind a shock wave front, Landerville *et al*. have performed density functional theory direct dynamics simulations setup by choosing molecular pairs colliding head on along specific crystallographic directions [100], [110], and [111] for PETN. The results show that each reactive collision case produces NO_2 as its first and major product.[34,35]

If the molecule evolves from the upper excited state (S_1) to the ground state, however, the $(S_1/S_0)_{CI}$ conical intersection becomes important, and the reaction path taken depends on a number of factors associated with the S_0 PES connecting to $(S_1/S_0)_{CI}$. Figure 7 (blue dotted line, arrow 3) directly indicates that, if the PETN molecule comes back to the ground state following the $(S_1/S_0)_{CI}$ CI, the most favorable path is associated with the nitro-nitrite isomerization, which is a barrierless channel. These paths are explicitly calculated using the IRC algorithm. The PETN molecule isomerizes to a nitrite form on its S_0 surface and then undergoes NO elimination, surmounting an energy barrier (~0.9 eV), to the NO elimination transition state. The force components on N and O atoms for the unstable normal mode of vibration for the NO elimination transition state ($S_{0,TS,NO\text{-}elimin}$) on the S_0 surface of PETN are almost parallel (see Fig. 8 "$S_{0,TS,NO\text{-}elimin}$"). This transition state is thereby predicted to produce little torque on the terminal NO moiety. Therefore, decomposition of the PETN molecule, following nonadiabatic relaxation through the $(S_1/S_0)_{CI}$ conical intersection followed by NO elimination on the ground state surface, is expected to produce a rotationally cold NO product. Additionally, following vertical excitation of PETN to its higher vibronic manifold of the S_1 surface, the molecule undergoes rapid nonadiabatic internal conversion from S_1 to S_0 through the $(S_1/S_0)_{CI}$ conical intersection and thereafter from the nitro-nitrite isomerization to NO elimination. Thus, on this pathway, the molecule stores significant electronic excitation energy in its vibrational degrees of freedom on the ground state surface. Moreover, compared to the bond length 1.21 Å of the NO at TS, the equilibrium bond length of the NO is about 1.14 Å, so there is a great chance to excite the vibration of NO. Based on the above discussion, a rotationally cold and vibrationally hot distribution of NO product from the S_0 surface is reasonable. Kuklja's group finds that 1,1-Diamino-2,2-dinitroethylene (DADNE) (Ref. 36) also produces a NO moiety from excited state decomposition, and produces a NO_2 moiety upon ground state decomposition, even though DADNE has a C–NO_2 bond, different from the O–NO_2 bond of PETN. X–NO_2 systems apparently have similar reaction mechanisms due to the presence of the NO_2 moiety.

VI. DISCUSSION

In this work, the energetic material PETN is studied both experimentally and theoretically to elucidate its decomposition pathways and initial fragmentation upon electronic state excitation. We have observed NO from the dissociation of PETN, and we conclude that it is the major initial product for its excited electronic state decomposition mechanism. In our experiments, the PETN parent molecule is excited to its first excited electronic state using different excitation wavelengths (226, 236, and 248 nm) that also correspond to the resonance transitions $A\ ^2\Sigma^+(\upsilon' = 0) \leftarrow X\ ^2\Pi(\upsilon'' = 0,1,2)$ of the NO molecule. The NO product from PETN displays similar cold rotational distributions (~20 K) at all three excitation wavelengths (226, 236, and 248 nm). Similar rovibronic spectral structures for the NO product from PETN at different excitation wavelengths indicate that the decomposition of PETN from its S_1 excited electronic state follows a single, excitation wavelength independent dissociation channel. Thus, we conclude that decomposition of the electronically excited energetic material PETN takes place through the same pathway at the three excitation wavelengths used in this experiment. Compared with the results for RDX, HMX, CL20, and others,[12–14] NO/NO_2/NO_3 containing energetic materials show similar NO product rovibronic distributions, that is, cold rotational and hot vibrational distributions. This behavior can be rationalized by the fact that PETN, and the other related NO/NO_2/NO_3 containing energetic molecules, must have similar and potentially characteristic dissociative excited state mechanisms, as described above, that all provide barrierless, single deactivation channels (e.g., $S_n \rightarrow S_{n-1} \rightarrow \ldots \rightarrow S_0$) for excited state initiated decomposition.

To get theoretical support and understanding for these experimental observations, the evolution pathways from excited electronic states with respect to the relevant reaction coordinates have to be known. We have, therefore, explored the PESs for PETN through the ONIOM(CASSCF:UFF) method (see Fig. 7). From calculation results, conical intersections are now firmly established to be the key features in the excited electronic state chemistry of the polyatomic molecules.[37–39] The concept of a conical intersection was first introduced by von Neumann and Wigner[40] and has now been recognized as essential for describing the dynamics and mechanisms for deactivation of a range of polyatomic molecules from their excited electronic states to their ground electronic PES.[41,42] One

of their most important implications is the rapid and efficient internal conversion from upper to lower electronic state surfaces through radiationless transitions. A radiationless transition through a conical intersection involves rapid conversion of electronic energy of the upper electronic state to vibrational energy (thermal energy) of the lower electronic state. As mentioned before, the excitation wavelengths used in our experiment correspond to the transition to the $S_1(n,\pi^*)$ excited state of the NO_2 moiety. Thus, for PETN, the energy of the $(S_1/S_0)_{CI}$ conical intersection is lower than the three excitation energies employed, which indicates that due to excitation to the $S_1(n,\pi^*)$ state, electronic energy can be rapidly thermalized through an almost barrierless nonadiabatic dissociation pathway from the FC point of the $S_1(n,\pi^*)$ state through the $(S_1/S_0)_{CI}$ conical intersection to the S_0 state PES. This dynamical process will generate NO product with cold rotational and hot vibrational distributions: the unstable normal mode of vibration associated with the relevant transition state on the ground electronic state surface does not generate a resultant torque on the NO moiety during dissociation of the parent molecule. This conclusion is in a good agreement with our experimental results.

Our previous research on nitramine and other energetic molecules[12–14,16,19] indicates that upon electronic excitation to the S_2 or S_1 state, the molecule follows a barrierless, most favorable descent pathway connecting the FC point of the S_2 or S_1 state to nitro-nitrite isomerization through the $(S_2/S_1)_{CI}$ and $(S_1/S_0)_{CI}$ CIs, and then gives rotationally cold and vibrationally hot NO product. Even though the N–NO_2 moiety is different from the O–NO_2 moiety, they both display a similar decomposition dynamics from the excited state, and obtain a similar experimental result (rotationally cold and vibrationally hot NO product). One reason for this similarity of behavior may be that with our chosen experimental wavelengths, excitations for O–NO_2 or N–NO_2 parent molecules are (n,π^*) states. Thus, they will have some similarities of PESs that may result in the similar barrierless, most favorable pathways for decomposition. The model system dimethylnitramine (DMNA) also has the N–NO_2 moiety, and the same (n,π^*) transitions for the first and second electronic excited states. But, in this instance, however, the NO product from DMNA displays hot rotational and cold vibrational energy distributions. Calculations reveal that DMNA, and other nonenergetic model systems,[13,27,28] decompose on their S_1 (or higher) electronically excited states rather than on their ground electronic states S_0; thereby, not all the excitation energy is available to break internal bonds to generate reactive fragments and radicals for further reactions, as may be required for true energetic behavior.

Combing all our previous experiments and theoretical calculations on energetic materials and model systems,[12–14,19,27] one can find that conical intersections play an important role in the decomposition mechanisms for both. The nitramine and related ($NO/NO_2/NO_3$) energetic materials all experience a NO elimination decomposition channel, and only generate a rotationally cold and vibrationally hot distribution of NO product. The decomposition dynamics are also similar for these species: the electronically excited energetic molecules follow a nonadiabatic relaxation to the ground state through a series of conical intersections, undergo a nitro-nitrite isomerization on the S_0 surface, followed by NO elimination. The model systems also give a NO product from their excited state decomposition, but the energy distribution for NO is not unique: some give rotationally hot and vibrationally cold distributions of NO, while some give rotationally cold and vibrationally hot distributions of NO. This behavior is excitation wavelength dependent. Therefore, these distinct results for energetic materials and model systems may be used in the future to predict, characterize, and distinguish energetic systems from nonenergetic or model systems.

VII. CONCLUSIONS

The excited electronic state decomposition of PETN has been investigated via nanosecond energy resolved spectroscopy. PETN generates NO as an initial decomposition product at the nanosecond laser excitation wavelengths (248, 236, 226 nm), and gives a hot vibrational (~1300 K) and cold rotational (~20 K) distributions of the NO product that are independent of excitation wavelengths. Based on the experimental observations and ONIOM combined with CASSCF calculations, we conclude that the decomposition of electronically excited PETN occurs through a barrierless overall most favorable descent, lowest energy pathway connecting the FC point of S_1 state to nitro-nitrite isomerization on S_0 through the $(S_1/S_0)_{CI}$ conical intersection, followed by NO elimination on S_0. Force components on N and O atoms for the unstable normal mode of vibration for the NO elimination transition state on the S_0 surface of PETN are predicted to produce little torque on the terminal NO moiety: this results in cold rotational (20 K) distributions of the NO product. On the contrary, if PETN molecule is thermally dissociated on the ground state surface only, the major decomposition channel should be O–NO_2 bond dissociation to yield the NO_2 product because this channel is associated with the lowest S_0 activation barrier.

According to our previous results on energetic materials and model systems, one may conclude: 1. decomposition of electronically excited NO_2 containing energetic materials occurs to yield NO product from their highly vibrationally excited S_0 states after following a series of conical intersections to their ground electronic states and 2. these molecules give rotationally cold and vibrationally hot distributions of NO. In the decomposition process, conical intersections play a crucial role in the initial decomposition mechanics for electronically excited energetic materials. In order to understand ultrafast internal conversion dynamics through the conical intersection, further investigation will be performed to study NO generation from PETN with ~100 fs time resolution.

ACKNOWLEDGMENTS

These studies were supported by a grant from the U.S. Army Research Office (ARO, FA9550-10-1-0454) and in part by the U.S. National Science Foundation (NSF) through TeraGrid supercomputer resources provided by NCSA under Grant No. TG-CHE090094. We thank Dr. Yuanqing Guo and Dr. Atanu Bhattacharya for many helpful discussions concerning the experiments and calculations for this system.

[1]J. Boileau, C. Fauquignon, B. Hueber, and H. H. Meyer, *Ullmann's Encyclopedia of Industrial Chemistry* (Wiley VCH, Berlin, 2000).
[2]M. F. Foltz, Report No. LLNL-TR-415057 (2009).
[3]D. Grewar, Can. Med. Assoc. J. **80**, 997 (1959); see online at http://www.ncbi.nlm.nih.gov/pmc/articles/PMC1831125/.
[4]V. Swayambunathan, G. Singh, and R. C. Sausa, Appl. Opt. **38**, 6447 (1999).
[5]C. S. Yoo, N. C. Holmes, P. C. Souers, C. J. Wu, F. H. Ree, and J. J. Dick, J. Appl. Phys. **88**, 70 (2000).
[6]C. J. Wu, F. H. Ree, and C.-S. Yoo, Propellants, Explos., Pyrotech. **29**, 296 (2004).
[7]A. C. Landerville, I. I. Oleynik, and C. T. White, J. Phys. Chem. A **113**, 12094 (2009).
[8]J.-S. Lee, C.-K. Hsu, and C.-L. Chang, Thermochim. Acta **392–393**, 173 (2002).
[9]C. M. Tarver, T. D. Tran, and R. E. Whipple, Propellants, Explos., Pyrotech. **28**, 189 (2003).
[10]P. S. Makashir and E. M. Kurian, Propellants, Explos., Pyrotech. **24**, 260 (1999).
[11]J. Budzien, A. P. Thompson, and S. V. Zybin, J. Phys. Chem. B **113**, 13142 (2009).
[12]Y. Q. Guo, M. Greenfield, A. Bhattacharya, and E. R. Bernstein, J. Chem. Phys. **127**, 154301 (2007).
[13]Y. Q. Guo, A. Bhattacharya, and E. R. Bernstein, J. Chem. Phys. **128**, 034303 (2008).
[14]A. Bhattacharya, Y. Q. Guo, and E. R. Bernstein, J. Chem. Phys. **131**, 194304 (2009).
[15]H. S. Im and E. R. Bernstein, J. Chem. Phys. **113**, 7911 (2000).
[16]Y. Q. Guo, M. Greenfield, and E. R. Bernstein, J. Chem. Phys. **122**, 244310 (2005).
[17]L. C. Snoek, T. Van Mourik, and J. P. Simons, Mol. Phys. **101**, 1239 (2003).
[18]P. Carcabal, R. T. Kroemer, L. C. Snoek, J. P. Simons, J. M. Bakker, I. Compagnon, G. Meijer, and G. V. Helden, Phys. Chem. Chem. Phys. **6**, 4546 (2004).
[19]A. Bhattacharya and E. R. Bernstein, J. Phys. Chem. A **115**, 4135 (2011).
[20]M. J. Frisch, G. W. Trucks, H. B. Schlegel *et al.*, GAUSSIAN 09, Revision A.1, Gaussian, Inc., Wallingford, CT, 2009.
[21]M. Svensson, S. Humbel, R. D. J. Froese, T. Matsubara, S. Sieber, and K. Morokuma, J. Phys. Chem. **100**, 19357 (1996).
[22]S. Humbel, S. Sieber, and K. Morokuma, J. Chem. Phys. **105**, 1959 (1996).
[23]T. Vreven and K. Morokuma, J. Comput. Chem. **21**, 1419 (2000).
[24]M. J. Bearpark, S. M. Larkin, and T. Vreven, J. Phys. Chem. A **112**, 7286 (2008).
[25]C. J. S. M. Simpson, P. T. Griffiths, H. L. Wallaart, and M. Towrie, Chem. Phys. Lett. **263**, 19 (1996).
[26]G. Herzberg, *Spectra of Diatomic Molecules* (Van Nostrand, New York, 1950), p. 257.
[27]A. Bhattacharya, Y. Q. Guo, and E. R. Bernstein, J. Phys. Chem. A **113**, 811 (2009).
[28]Y. Q. Guo, A. Bhattacharya, and E. R. Bernstein, J. Phys. Chem. A **113**, 85 (2008).
[29]Y. A. Gruzdkov and Y. M. Gupta, J. Phys. Chem. A **105**, 6197 (2001).
[30]I. Borges, Jr., A. J. A. Aquino, M. Barbatti, and H. Lischka, Int. J. Quantum Chem. **109**, 2348 (2009).
[31]W. Flicker, J. Chem. Phys. **72**, 2788 (1980).
[32]M. J. McQuaid and R. C. Sausa, Appl. Spectrosc. **45**, 916 (1991).
[33]P. Celani, M. A. Robb, M. Garavelli, F. Bernardi, and M. Olivucci, Chem. Phys. Lett. **243**, 1 (1995).
[34]A. Landerville, I. I. Oleynik, M. A. Kozhushner, and C. T. White, AIP Conf. Proc. **955**, 447 (2007).
[35]A. C. Landerville, I. I. Oleynik, and C. T. White, AIP Conf. Proc. **1195**, 813 (2009).
[36]A. V. Kimmel, P. V. Sushko, A. L. Shluger, and M. M. Kuklja, J. Chem. Phys. **126**, 234711 (2007).
[37]G. A. Worth and L. S. Cederbaum, Annu. Rev. Phys. Chem. **55**, 127 (2004).
[38]W. Domcke, D. R. Yarkony, and H. Koppel, *Conical Intersections: Electronic Structure, Dynamics and Spectroscopy* (World Scientific, River Edge, NJ, 2003).
[39]M. Baer and G. D. Billing, *The Role of Degenerate States in Chemistry: Advances in Chemical Physics* (Wiley, Hoboken, NJ, 2002), Vol. 124, p. 124.
[40]J. von Neumann and E. Wigner, Z. Phys. **49**, 73 (1928).
[41]J. Soto, J. F. Arenas, J. C. Otero, and D. Peláez, J. Phys. Chem. A **110**, 8221 (2006).
[42]L. Blancafort, J. Am. Chem. Soc. **128**, 210 (2005).